(2)

NAVAL POSTGRADUATE SCHOOL

Monterey, California

THESIS

COMPUTER SIMULATION OF GOLD CODE PHASE MODULATION IN OCEAN ACOUSTIC TOMOGRAPHY

By

Peter James Lynch

June 1989

Thesis Advisor: James H. Miller

UNCLASSIFIED
SECURITY CLASSIFICATION OF THIS PAGE

REPORT DOCUMENTATION PAGE

Form Approved OMB No. 0704-0188

1a REPORT SECURITY CLASSIFICATION	1b RESTRICTIVE MARKINGS
2a SECURITY CLASSIFICATION AUTHORITY	3 DISTRIBUTION/AVAILABILITY OF REPORT: Approved for public release; distribution is unlimited.
2b DECLASSIFICATION/DOWNGRADING SCHEDULE	
4 PERFORMING ORGANIZATION REPORT NUMBER(S)	5 MONITORING ORGANIZATION REPORT NUMBER(S)
6a NAME OF PERFORMING ORGANIZATION: Naval Postgraduate School	6b OFFICE SYMBOL (If applicable): 62
7a NAME OF MONITORING ORGANIZATION: Naval Postgraduate School	
6c ADDRESS (City, State, and ZIP Code): Monterey, CA 93943-5000	7b ADDRESS (City, State, and ZIP Code): Monterey, CA 93943-5000
8a NAME OF FUNDING/SPONSORING ORGANIZATION	8b OFFICE SYMBOL (If applicable)
8c ADDRESS (City, State, and ZIP Code)	9 PROCUREMENT INSTRUMENT IDENTIFICATION NUMBER
	10 SOURCE OF FUNDING NUMBERS: PROGRAM ELEMENT NO; PROJECT NO; TASK NO; WORK UNIT ACCESSION NO

11 TITLE (Include Security Classification)
COMPUTER SIMULATION OF GOLD CODE PHASE MODULATION IN OCEAN ACOUSTIC TOMOGRAPHY

12 PERSONAL AUTHOR(S)
LYNCH, Peter James

13a TYPE OF REPORT	13b TIME COVERED	14 DATE OF REPORT (Year, Month, Day)	15 PAGE COUNT
Master's Thesis	FROM ____ TO ____	June 1989	61

16 SUPPLEMENTARY NOTATION: The views expressed in this thesis are those of the author and do not reflect the official policy or position of the Department of Defense or the US Government.

17 COSATI CODES: FIELD	GROUP	SUB-GROUP	18 SUBJECT TERMS (Continue on reverse if necessary and identify by block number): Acoustic, Tomography, Gold codes, Arrival times

19 ABSTRACT (Continue on reverse if necessary and identify by block number)

This work investigates the viability of Gold code phase modulation in acoustic tomography, a technique for large scale measurement of ocean characteristics. Maximal-length sequences are currently used for modulation, requiring time division multiplexing of tomographic signals to avoid interference. The proposed alternative scheme of code division multiplexing Gold code modulated signals promises more rapid, simultaneous ocean projections. Computer simulation enables side-by-side comparison of the Gold code and maximal-length sequence modulating methods. Based on favorable results, a specific set of Gold codes is recommended for future use in a tomography experiment. Thesis (RY

20 DISTRIBUTION/AVAILABILITY OF ABSTRACT	21 ABSTRACT SECURITY CLASSIFICATION
☒ UNCLASSIFIED/UNLIMITED ☐ SAME AS RPT ☐ DTIC USERS	UNCLASSIFIED
22a NAME OF RESPONSIBLE INDIVIDUAL: James H. Miller	22b TELEPHONE (Include Area Code): (408)646-2384 / 22c OFFICE SYMBOL: 62MR

DD Form 1473, JUN 86 ____ UNCLASSIFIED

Approved for public release; distribution is unlimited.

Computer Simulation of Gold Code Phase Modulation in Ocean Acoustic Tomography

by

Peter James Lynch
Lieutenant, United States Navy
B.S., Massachusetts Institute of Technology, 1981

Submitted in partial fulfillment of the requirements for the degree of

MASTER OF SCIENCE IN ELECTRICAL ENGINEERING

from the

NAVAL POSTGRADUATE SCHOOL
June 1989

Author: 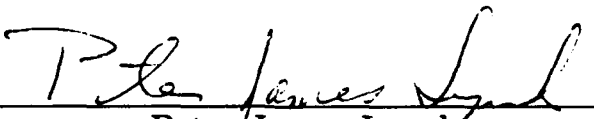
Peter James Lynch

Approved by: 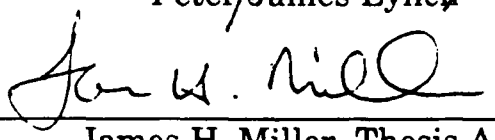
James H. Miller, Thesis Advisor

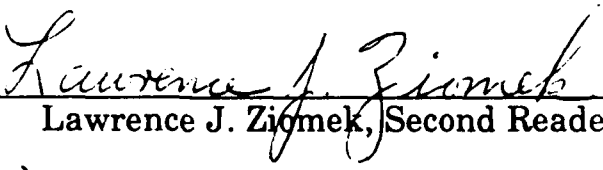
Lawrence J. Ziomek, Second Reader

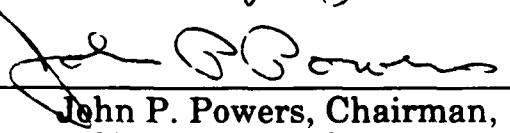
John P. Powers, Chairman,
Department of Electrical and Computer Engineering

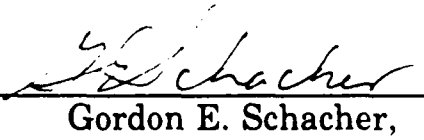
Gordon E. Schacher,
Dean of Science and Engineering

ABSTRACT

This work investigates the viability of Gold code phase modulation in acoustic tomography, a technique for large scale measurement of ocean characteristics. Maximal-length sequences are currently used for modulation, requiring time division multiplexing of tomographic signals to avoid interference. The proposed alternative scheme of code division multiplexing Gold code modulated signals promises more rapid, simultaneous ocean projections. Computer simulation enables side-by-side comparison of the Gold code and maximal-length sequence modulating methods. Based on favorable results, a specific set of Gold codes is recommended for future use in a tomography experiment.

TABLE OF CONTENTS

LIST OF TABLES

LIST OF FIGURES

I. INTRODUCTION

Present-day ocean acoustic tomography relies on time division multiplexing of signals [Refs. 1,2,3]. Simultaneous transmissions have not been used for essentially two reasons:

1. for multiple sources transmitting carriers phase modulated with the same m-sequence, ambiguity would exist as to which source transmitted a given detected signal [Refs. 2,3]; and
2. for sources transmitting carriers modulated with different m-sequences, spurious arrivals caused by sequence cross-correlation peaks could easily be mistaken for genuine multipath arrivals.

This work investigates the possibility of code division multiplexing tomographic signals. Gold code phase modulation has the advantage of uniquely identifying each transmitted signal by its code, eliminating ambiguity [Refs. 4,5]. Additionally, due to Gold codes' low crosscorrelation, spurious arrival peaks can be reduced.

In all acoustic tomography work to date, travel time deviation is the key parameter measured. The time and space-dependent variations from an anticipated travel time become the basis for inferring ocean characteristics through mathematical inverse analysis. Classical impulse-type acoustic sources (such as explosions) tend to suffer great attenuation and time spreading during ocean acoustic travel, as shown in Figure 1. Additionally the presence of noise makes accurate travel time determination even more challenging. It is for these reasons that acoustic tomography has

resorted to signals frequency-spread by phase modulation with maximal-length sequences [Ref. 2]. As will be shown in Chapter II, such modulation schemes achieve tremendous processing gain through pulse compression, making accurate travel time measurements achievable.

The purpose of this work is to explore alternative sequences for tomography signal phase modulation. Specific objectives in this pursuit are to prove (or disprove) that Gold codes will enable simultaneous signal transmission without significant degradation of travel time determination capability. If achievable, the advantages of this approach over the time division multiplexing scheme currently employed are:

1. improvement in data gathering rate by a factor of R where R is the number of signals simultaneously transmitted;
2. enables accurate velocity tomography measurements to be made with simultaneous to-and-fro shots at numerous projection angles; and
3. hands-off operation, eliminating timing and logistical problems associated with moving or switching transmitters and receivers.

An additional objective of this work is to recommend a specific set of codes for future use in a simultaneous transmission tomography experiment.

In the succeeding chapters this work will be described as follows:

1. background on maximal-length sequences and Gold codes and their properties;
2. description of computer simulation of Gold codes versus m-sequences in single signal tomography;

3. description of computer simulation of Gold codes versus m-sequences in multi-signal tomography; and
4. results, conclusions, summary, and recommendations.

II. M-SEQUENCES AND GOLD CODES

Maximal length sequences are generated by certain linear feedback shift register (LFSR) configurations derived from finite field arithmetic. Without getting into great detail on finite field theory, the basic concepts will now be presented.

Polynomials which cannot be expressed as a product of lower order polynomials are referred to as irreducible polynomials [Ref. 6]. A subset of irreducible polynomials of interest is the set of primitive polynomials. Primitive polynomials p(x) of degree m possess the characteristic that the smallest integer n for which p(x) divides

$$r = x^n + 1 \qquad (1)$$

evenly is

$$n = 2^m - 1 \qquad (2)$$

Primitive polynomials can be realized in hardware in the form of shift registers with linear feedback connections through exclusive-or gates. Such constructions generate m-sequences, periodic binary codes with certain unique properties. A signal designer in search of an m-sequence must therefore first find its corresponding primitive polynomial, a potentially nontrivial pursuit. Fortunately, many have done this before and the way has been paved. Tables of primitive

polynomials up to very high order are in the literature [Refs. 6,7], so the signal designer need only choose from the published list for the order polynomial required. Polynomials in these tables are, by convention, presented in octal format, so as to easily fit on a printed page. An example is in order to demonstrate how one arrives at the LFSR design given a typical table entry.

EXAMPLE:

An m-sequence of length 511 (2^9 -1) is desired. From the table of primitive polynomials the entry 1461 is chosen.

Step 1: The entry is rewritten in binary coded decimal (BCD) as follows:

octal	1	4	6	1
BCD	001	100	110	001 .

Step 2: The primitive polynomial is normally written in powers of D rather than x to emphasize feedback delay. Its coefficients are either 1 or 0 as appropriate in the binary code, with the rightmost bit considered least significant (i.e., the rightmost bit becomes the coefficient of D^0).

$$p(D) = 1 + D^4 + D^5 + D^8 + D^9 \qquad (3)$$

Step 3: A LFSR reflecting the appropriate delays fed back is constructed, here shown in Figure 2. Given any initial load (except all zeros, an illegal state) this LFSR will output a single m-sequence repetitively as the clock continually shifts bits through. Different initial loads will not change the output; they will produce a shifted version of the same m-sequence. As a side note it should be added that, due to the possibility of the illegal all zeros state occurring, the LFSR should have a detection/correction mechanism for this eventuality.

Several properties peculiar to maximal length sequences will now be noted:

1. Periodic Property. The period N of an m-sequence is

$$N = 2^n - 1 \qquad (4)$$

where n is the number of stages in the shift register generator.

2. Balance Property. The total number of ones in one period of an m-sequence is

$$\frac{1}{2}(N + 1) = 2^{n-1} \qquad (5)$$

and the total number of zeros is

$$\frac{1}{2}(N - 1) = 2^{n-1} - 1 \qquad (6)$$

3. Window Property. A sliding window of width n bits will contain every possible combination of ones and zeros (except all zeros) as it is shifted through the repeated sequence.
4. Run Length Property. For any m-sequence there is exactly:

    1. 1 run of ones of length n
    2. 1 run of zeros of length n-1
    3. 1 run of ones and one run of zeros of length n-2
    4. 2 runs of ones and 2 runs of zeros of length n-3
    5. 4 runs of ones and 4 runs of zeros of length n-4
    .
    .
    .
    n. 2^{n-3} runs of ones and 2^{n-3} runs of zeros of length 1.

5. **Shift-and-Add Property.** The digit-by-digit binary sum (no carries) of an m-sequence and any shift of that same sequence is another shift of the sequence.
6. **Autocorrelation Property.** The periodic autocorrelation function $\theta_b(n)$ of any m-sequence is two-valued and given by

$$\theta_b(n) = \left\{ \begin{array}{ll} N, & n = jN \\ -1, & \text{otherwise} \end{array} \right\}. \qquad (7)$$

[Refs. 6,8]

As Equation 7 and Figure 3 indicate, maximal length sequences possess single high-peaked periodic autocorrelation functions with no sidelobes. The magnitude of such correlation functions equals N (the sequence length) at zero shift and +1 elsewhere. Correlation can be regarded as a measure of similarity. Therefore, the m-sequence autocorrelation characteristic indicates that any shifted version of an m-sequence matches the original sequence very poorly, while the unshifted sequence matches itself exactly. It is this property which renders m-sequences so useful for tomography. The transmitted tomographic signal

$$A\cos[\, 2\pi f_o t + \theta(t)\,] \qquad (8)$$

arrives attenuated, noise-corrupted, and phase-shifted at the receiver as

$$B\cos[\, 2\pi f_o t + \theta(t) + \phi\,] + n(t) \qquad (9)$$

Here B is the initial amplitude A attenuated along the acoustic path, and

$$\phi = -2\pi f_o \tau \qquad \{10\}$$

represents the phase shift of the sinusoid caused by travel time τ. When correlating the received signal of Equation 9 with the m-sequence used for modulation, the horizontal displacement of the correlation peak corresponds to the travel time delay for that signal.

Although m-sequence autocorrelation properties are widely known and exploited, their crosscorrelation characteristics are often overlooked. If one considers transmitting not one but several signals simultaneously, the interference between these signals will be related to their periodic crosscorrelations. The signal designer's objective should therefore be to minimize crosscorrelations while maximizing autocorrelation peaks of the modulating sequences.

M-sequence crosscorrelation functions are multiple-valued. Additionally, they depend on the particular pair of sequences chosen. For a specific case with N=127, a crosscorrelation function is shown in Figure 4. Certain pairs of m-sequences can be found with three-valued, minimum crosscorrelations. Such sequences, denoted preferred pairs, have crosscorrelations which take on one of the following values:

$$\theta_c(n) = \left\{ \begin{array}{l} t(n) \\ -1 \\ t(n) - 2 \end{array} \right\} \qquad (11)$$

where

$$t(n) = \left\{ \begin{array}{ll} 1 + 2^{\frac{1}{2}(n+1)}, & n \text{ odd} \\ 1 + 2^{\frac{1}{2}(n+2)}, & n \text{ even}, n \neq \text{mod } 4 \end{array} \right\}, \qquad (12)$$

as can be observed in Figure 5 for N =127.

Preferred pairs are the best among all m-sequences in terms of minimizing crosscorrelation interference while maintaining high single-peaked autocorrelations. They should be good choices for phase modulation in multi-signal tomography. Sets of sequences containing all mutually-preferred pairs are called maximal connected sets. Unfortunately, for any given sequence length, there are only a handful M_n of preferred pairs in each maximal connected set. Only a handful of signals could therefore be modulated and transmitted with minimum interference, thus limiting the utility of preferred pairs for multi-signal tomography when more than a few signals are to be simultaneously transmitted.

Table 1 shows set sizes and crosscorrelation bounds for the sets of all m-sequences and for maximal connected sets. The superiority of preferred pairs in crosscorrelation characteristics over random m-

sequences increases with n, at least through n=14, which represents a sequence length of 16383 [Ref. 10].

For applications requiring large groups of signals with low crosscorrelation bounds, some hybrid of preferred pairs which preserves their crosscorrelation properties but includes many sequences is desirable. Sets of Gold codes possess just such characteristics.

Any preferred pair of m-sequences becomes the first two Gold codes in a complete set of N + 2. The remaining N sequences can be analytically constructed through bit-by-bit binary addition (no carries) of one member of the preferred pair with all possible circular shifts of the other. This operation is easily implemented in hardware with an exclusive-or operation on the outputs of the LFSRs generating the two preferred pairs. Each Gold code in the resulting set of N + 2 possesses the same low three-valued crosscorrelation with all other sequences in the set, shown in Figure 6 for N=127. This makes them well-suited for multi-signal applications where low intersignal interference is required. Unfortunately, although the Gold code crosscorrelations are the same as preferred pairs of m-sequences, their autocorrelations are not. Only the initial preferred pair in each Gold code set are m-sequences and possess their single-peaked autocorrelation. The remaining N Gold codes are not m-sequences. Of all the m-sequence properties, only Properties 1 and 2 hold true for these remaining Gold codes. Of particular interest are their autocorrelation properties.

Although these Gold codes still possess high-peaked autocorrelations, unlike m-sequences they have sidelobes with maximum level

$$\theta_c = t(n) . \qquad \{13\}$$

Note from Table 1 that for N=127 the value of t(n) is 17. As expected, this is precisely the maximum Gold code autocorrelation sidelobe level shown in Figure 7.

Clearly there is a tradeoff between autocorrelation peaks and sidelobe levels for sets of sequences. A theoretical relationship is

$$\left(\frac{\theta_c^2}{N}\right) + \frac{N-1}{N(K-1)}\left(\frac{\theta_a^2}{N}\right) \geq 1 \qquad \{14\}$$

where θ_c is the maximum periodic crosscorrelation magnitude, θ_a is the maximum out-of-phase periodic autocorrelation magnitude, N is the sequence length , and K is the number of sequences in the set. [Ref. 10]

III. SIMULATION OF SINGLE-SIGNAL TOMOGRAPHY

A. MODEL DESCRIPTION

In an actual tomography experiment, the received signal of Equation 9 is initially bandpass filtered to remove any noise outside the signal bandwidth. Next, as shown in Figure 8, the signal is power divided and passed through a quadrature demodulator. At this point , lowpass filtering passes the difference frequency only, blocking the sum at twice the carrier frequency. After sampling above the Nyquist rate, the received signal is reduced to a set of filtered, discrete samples. By correlating these samples with the original modulating sequence, a peak is obtained whose horizontal position on the time scale corresponds to deviation of the acoustic signal arrival time from the assumed or predicted value. Inverse theory transforms such travel time deviations from various projections to a matrix of ocean densities, the quantities sought.

In the computer model, approximations have been made to actual experimental technique and ocean phenomena. Noise which is assumed to be originally additive, white, and Gaussian, after bandlimiting by the front end bandpass filter, takes on other properties. From the theory of narrowband random processes, it can be shown that at the output of the correlator receiver, the in-phase and quadrature components of noise are related by a Hilbert transform [Ref. 11].

The in-phase and quadrature channel noise samples are obtained by digital Hilbert transforming and lowpass digital filtering a vector of normally distributed samples with zero mean and prescribed variance.

Time-delayed in-phase and quadrature signal samples are generated by FORTRAN code, then passed through the digital lowpass filter. By summing the appropriate noise and signal samples, the in-phase and quadrature baseband received signals are approximated in the simulation. Signal-to-noise ratio (SNR) is varied by fixing the Gaussian noise sample variance and changing signal amplitudes accordingly. Relative phase is adjusted with signal time delay. In order to compare m-sequences to Gold codes, they are tested side-by-side under identical conditions of SNR and signal delay. Sidelobe levels on the final correlation are the quantities used for comparison. Correlation with the modulating sequence is calculated by means of Discrete Fourier Transforms (DFTs).

B. PROCEDURE

This computer simulation was tailored after velocity tomography experiments conducted in 1984. Sequence lengths of 511 digits modulate a 400 Hz carrier. Digit durations of .01 seconds produce a signal period of 5.11 seconds [Ref. 2].

The m-sequences or Gold codes to be used for signal modulation were first generated with appropriate LFSR configurations. The LFSRs are based on the octals 1021 and 1751, selected from the tables of primitive polynomials [Refs. 6,7]. The binary (0,1) sequences

produced were mapped to (1,-1) sequences, then used to phase modulate the carrier with angle

$$\theta_m = \tan^{-1}(\sqrt{N}). \qquad (15)$$

[Ref. 2]

Baseband in-phase and quadrature signal components were generated as the cosine and sine of this modulating angle. The signals were sampled twice per digit, resulting in 1022 samples each for the in-phase and quadrature channels. To simulate an actual received signal, noise samples were added and the result lowpass filtered.

Noise samples were created by first generating a vector of 1100 normally distributed samples with zero mean and variance of 0.25. These samples were passed through a 19th-order digital Hilbert transformer with frequency response shown in Figures 9 and 10 and filter coefficients listed in Table 2 [Refs. 12,13]. Design of this filter is discussed in Appendix C. The filter input and output vectors represent in-phase and quadrature noise components, respectively. After adding these noise samples to the appropriate in-phase and quadrature signal samples generated above, lowpass filtering was performed. For this operation, an 8th-order Butterworth digital filter with a 3 dB cutoff frequency of 90 Hz was employed. Its frequency response is shown in Figures 11 and 12, with filter coefficients listed in Table 3 [Refs. 12,13], and design discussion in Appendix D [Ref. 13].

The output samples of this filter represent the in-phase and quadrature received signal-plus-noise samples. From these 1100 samples, the 1022 center samples were extracted to avoid end fringe effects. This simulates one full period of samples in a periodic stream. These samples were next correlated with 1022 code samples. The periodic or circular correlation of 1022 received signal samples with 1022 samples of the modulating binary (+1,-1) code can be performed in several different ways. The method used in this simulation was correlation by DFTs. Let the received signal samples be $x_r(n)$ and the binary code samples be $x_c(n)$. Both sequences are the same length, as is required for circular correlation. The periodic correlation of these two sequences itself repeats with period 1022. If X(k) is used to denote the DFT of x(n),

$$X(k) = \sum_{n=0}^{1021} x(n) e^{-j\left(\frac{2\pi}{1022}\right)nk} \quad . \qquad (16)$$

Then the periodic correlation of the sequences $x_r(n)$ and $x_c(n)$ is given by an Inverse Discrete Fourier Transform (IDFT):

$$x_0(n) = \mathrm{IDFT}\left[X_r^*(k)\, X_c(k)\right] \quad . \qquad (17)$$

[Ref. 13]

Sidelobe levels of this correlation are compared for m-sequence and Gold code modulation as a measure of their relative merit.

C. RESULTS

Figures 13 and 14 show the key results for a SNR=0 dB, a typical region of operation for tomography. Maximum sidelobes for the m-sequence correlations are at -35 dB, while for Gold codes the maximum sidelobes are at -21 dB.

Maximal-length sequences outperformed Gold codes in single-signal tomography, and this comes as no surprise. The two-valued autocorrelation of m-sequences is optimal, and since there is no second signal to act as a jammer, crosscorrelation properties are not significant.

IV. SIMULATION OF MULTIPLE-SIGNAL TOMOGRAPHY

A. MODEL DESCRIPTION

The computer simulation for multi-signal tomography is identical to that described in Chapter III for single-signal tomography, with one exception. In this simulation, a jamming tomographic signal is added using a different m-sequence or Gold code from the transmitted signal of interest. For a fair comparison, an average m-sequence is chosen to modulate the m-sequence jammer. This m-sequence has a peak crosscorrelation value of 95 with the primary modulating m-sequence, as compared with a possible worst case of 113 (see Table 1) or the best case of 33 if the preferred pair had been chosen.

B. PROCEDURE

The jamming sequences used were, as before, generated by LFSRs constructed from octals picked from the table of primitive polynomials described in Chapter II [Refs. 6,7]. Amplitudes of the corresponding jamming signals were adjusted relative to the intended signal amplitude to give the signal-to-jammer ratio (SJR) desired. The jammer, in a process identical to that used for the primary signal, was reduced to in-phase and quadrature samples. These samples, when added to the corresponding signal-plus-noise samples, produced samples of signal-plus-interference-plus-noise. After lowpass filtering, correlation with the primary modulating sequence was performed as

described in Chapter III. Following correlation with the original sequence, maximum sidelobe levels were compared for m-sequence versus Gold code modulation.

C. RESULTS

Correlations for no noise and SJR=0 dB can be compared in Figures 15 and 16. These results show maximum sidelobes for Gold codes 6.3 dB lower than those for m-sequence modulation. As SNR decreases, however, this advantage shrinks. For SNR=0 dB and SJR=0 dB, a likely scenario for tomography, the Gold code sidelobe advantage shrinks to 2 dB, as shown in Figures 17 and 18. The Gold code performance improvement is therefore accompanied by increased susceptibility to noise.

V. CONCLUSIONS

This work has explored the performance of Gold codes in phase modulating ocean acoustic tomography signals. The following conclusions and recommendations are based on results obtained from computer simulation of one specific modulating arrangement (using 511-digit modulating sequences and 90 Hz bandwidth signals) only. Therefore, our results strictly apply to only this particular configuration. Any theories extending beyond this work will require validation through additional research. However, this work does show that Gold codes can be used to advantage in ocean acoustic tomography.

As predicted by theory, m-sequences outperform Gold codes in single-signal tomography due to their two-valued autocorrelation function. Gold code autocorrelation sidelobes reduce the pulse compression processing gain available by 14 dB in this simulation operating near a SNR=0 dB. However, as sequence length increases beyond 511, the Gold code sidelobe levels drop, and their performance in single-signal tomography will improve.

The multiple-signal tomography simulation results are not so straightforward to analyze. For a 0 dB interference level, 511-digit Gold codes show a 6.3 dB advantage in a no-noise environment, diminishing to a 2 dB advantage as the SNR decreases to zero. The key m-sequence results in Figures 15 and 17 show an insensitivity of the m-sequence modulating scheme to noise. Note that there is almost

no change in sidelobes between the no-noise situation and the SNR=0 dB arrangement. By contrast, Gold code results in Figures 16 and 18 show appreciable performance degradation as the SNR is reduced. A theory which accounts for this disparity is again related to the autocorrelation sidelobes and sequence lengths. This theory follows: correlation, which is tomography's travel time measuring tool, is a product of shifted signals-plus-noise. If one regards the autocorrelation and crosscorrelation functions of the modulating sequences as temporal filters in series, note that noise is passed where both filters have sidelobes. Since m-sequences have autocorrelation sidelobes of magnitude 1/N , virtually no noise passes. In contrast, Gold codes' three-valued crosscorrelations are appreciable, although small at sequence lengths of 511. When these peaks line up with autocorrelation sidelobe peaks, noise is passed. However, if the modulating sequence length is increased, relative sidelobe levels should decrease, making Gold codes more noise-resistant. Gold codes of 511-digits offer the best performance in multi-signal tomography at very low signal-to-noise ratios. Their advantage varies with SNR, from 6.3 dB with no noise to 2 dB for SNR near 0 dB. The answer is to utilize these shorter Gold codes whenever possible with as much signal power as is feasible to maximize their advantage. Future tomography experiments could try out Gold codes as a logistics saving technique. An ideal application would be in a velocity tomography experiment, in which simultaneous transmissions contribute greatly to the accuracy of the results. Additionally, use of longer Gold sequences should be

explored due to the downward trend of maximum crosscorrelation with increasing sequence length discussed above.

APPENDIX A. TABLES

TABLE 1. SET SIZES AND CROSSCORRELATION BOUNDS FOR M-SEQUENCES AND FOR MAXIMAL CONNECTED SETS. [REF. 9]

n	$N = 2^n - 1$	Number of m-sequences	θ_c for set of all m-sequences	M_n	t(n)
3	7	2	5	2	5
4	15	2	9	0	9
5	31	6	11	3	9
6	63	6	23	2	17
7	127	18	41	6	17
8	255	16	95	0	33
9	511	48	113	2	33
10	1023	60	383	3	65
11	2047	176	287	4	65
12	4095	144	1407	0	129
13	8191	630	$\geq$ 703	4	129
14	16383	756	$\geq$ 5631	3	257
15	32767	1800	$\geq$ 2047	2	257
16	65535	2048	$\geq$ 4095	0	513

TABLE 2. 19TH-ORDER HILBERT TRANSFORMER COEFFICIENTS.

$$H(z) = a_0 + a_1 z^{-1} + \ldots + a_{19} z^{-19}$$

where:

$$a_0 = .01603$$
$$a_1 = .01417$$
$$a_2 = .02045$$
$$a_3 = .02874$$
$$a_4 = .03985$$
$$a_5 = .05533$$
$$a_6 = .07584$$
$$a_7 = .11824$$
$$a_8 = .20664$$
$$a_9 = .63476$$
$$a_{10} = -.63476$$
$$a_{11} = -.20664$$
$$a_{12} = -.11824$$
$$a_{13} = -.07854$$
$$a_{14} = -.05533$$
$$a_{15} = -.03985$$
$$a_{16} = -.02874$$
$$a_{17} = -.02045$$
$$a_{18} = -.01417$$
$$a_{19} = -.01603$$

TABLE 3. 8TH-ORDER BUTTERWORTH DIGITAL LOWPASS FILTER COEFFICIENTS.

$$H(z) = \frac{a_o + a_1 z^{-1} + \ldots + a_8 z^{-8}}{1 + b_1 z^{-1} + b_8 z^{-8}}$$

where:

$a_0 = .445085$

$a_1 = 3.56068$

$a_2 = 12.46238$

$a_3 = 24.92476$

$a_4 = 31.15595$

$a_5 = 24.92476$

$a_6 = 12.46238$

$a_7 = 3.56068$

$a_8 = .445085$

$b_1 = 6.390364$

$b_2 = 18.00034$

$b_3 = 29.17112$

$b_4 = 29.73142$

$b_5 = 19.5057$

$b_6 = 8.041041$

$b_7 = 1.903687$

$b_8 = .198103$

APPENDIX B. FIGURES

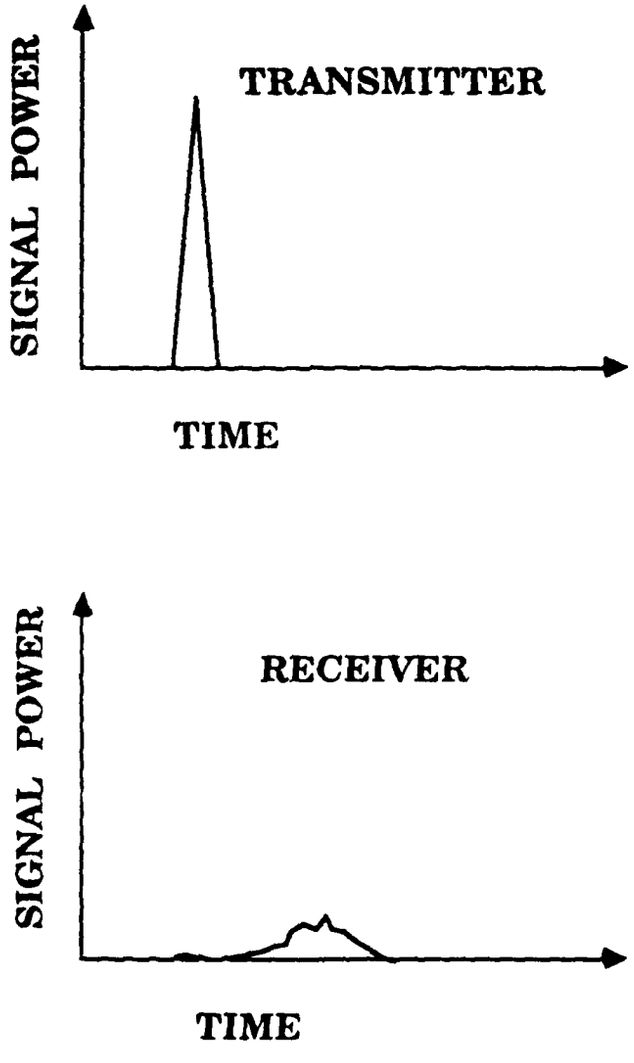

Figure 1. Pulse Spreading and Attenuation.

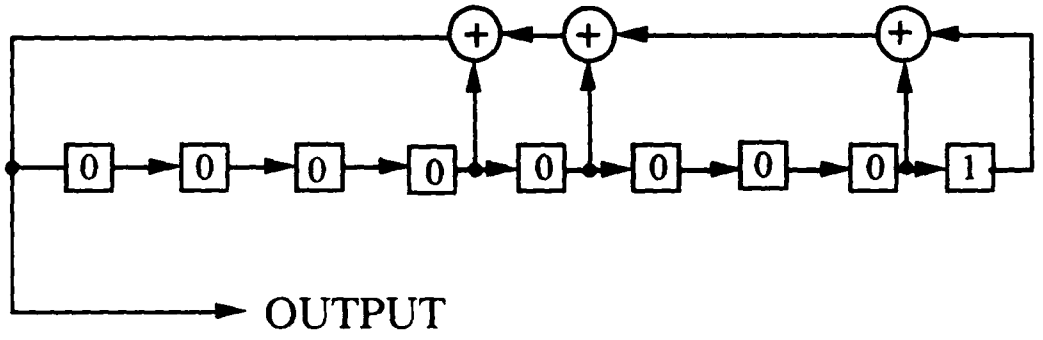

Figure 2. LFSR Realization of Octal 1461.

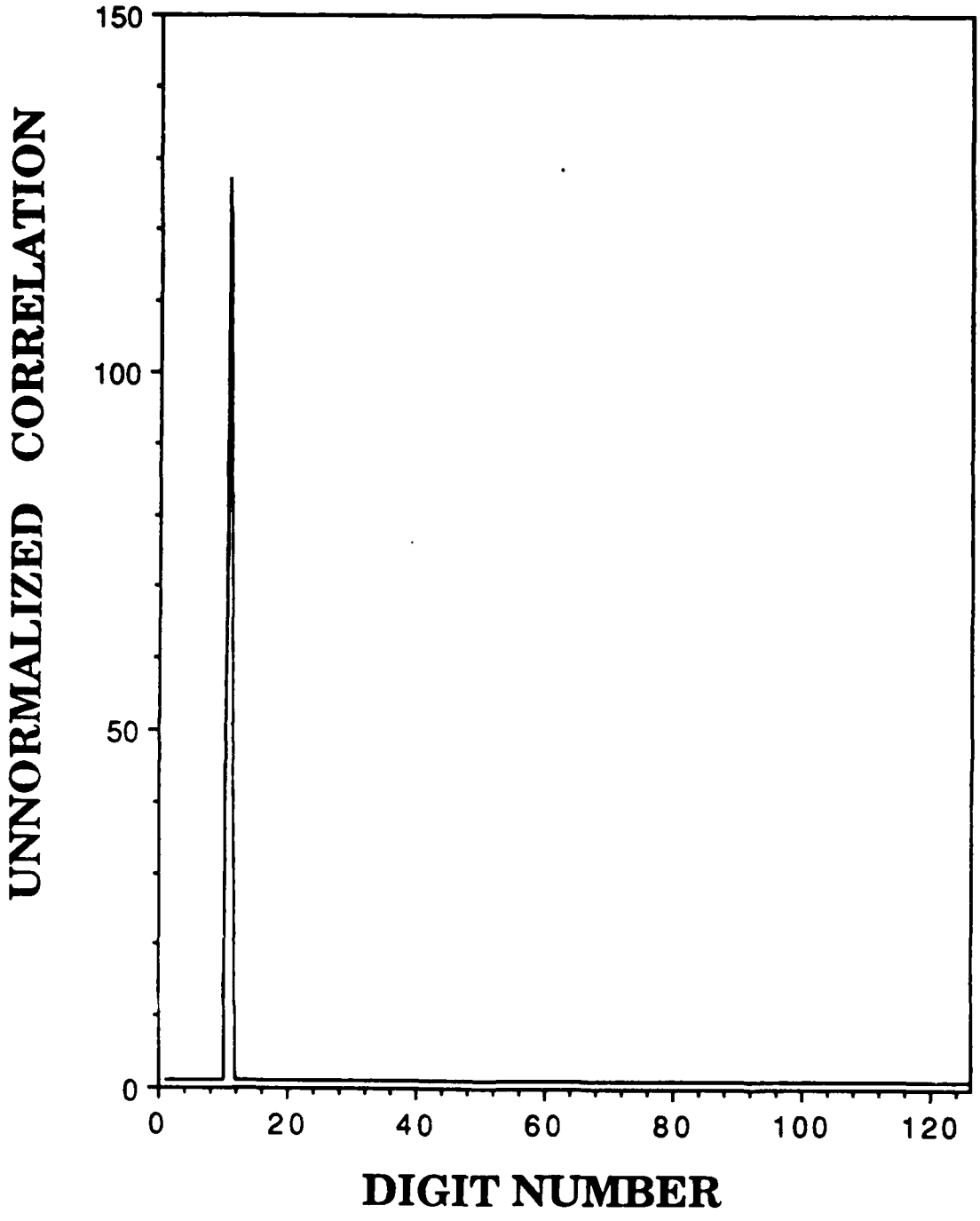

Figure 3. M-Sequence Autocorrelation for N=127.

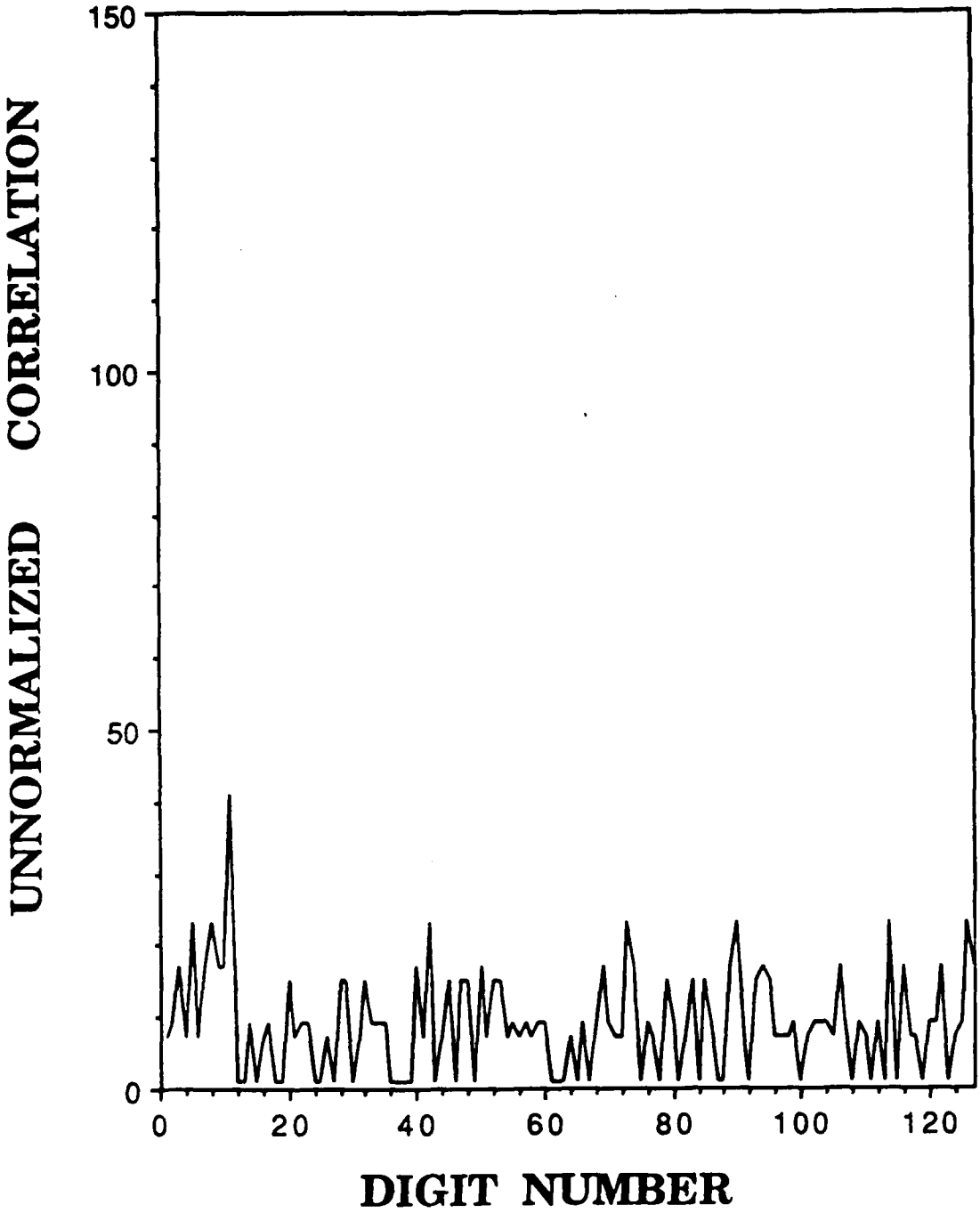

Figure 4. Typical M-Sequence Crosscorrelation, N=127.

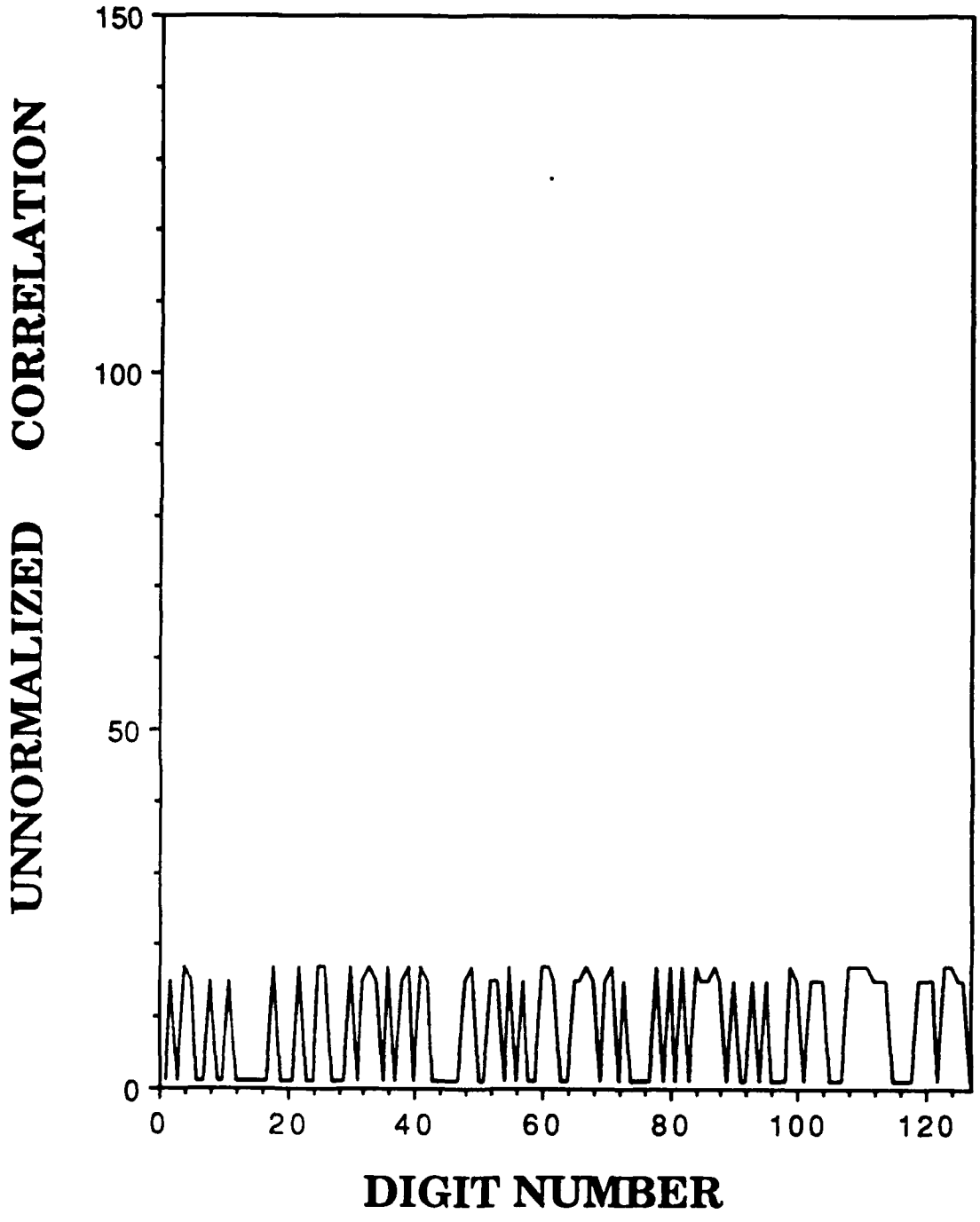

Figure 5. Preferred Pair Crosscorrelation, N=127.

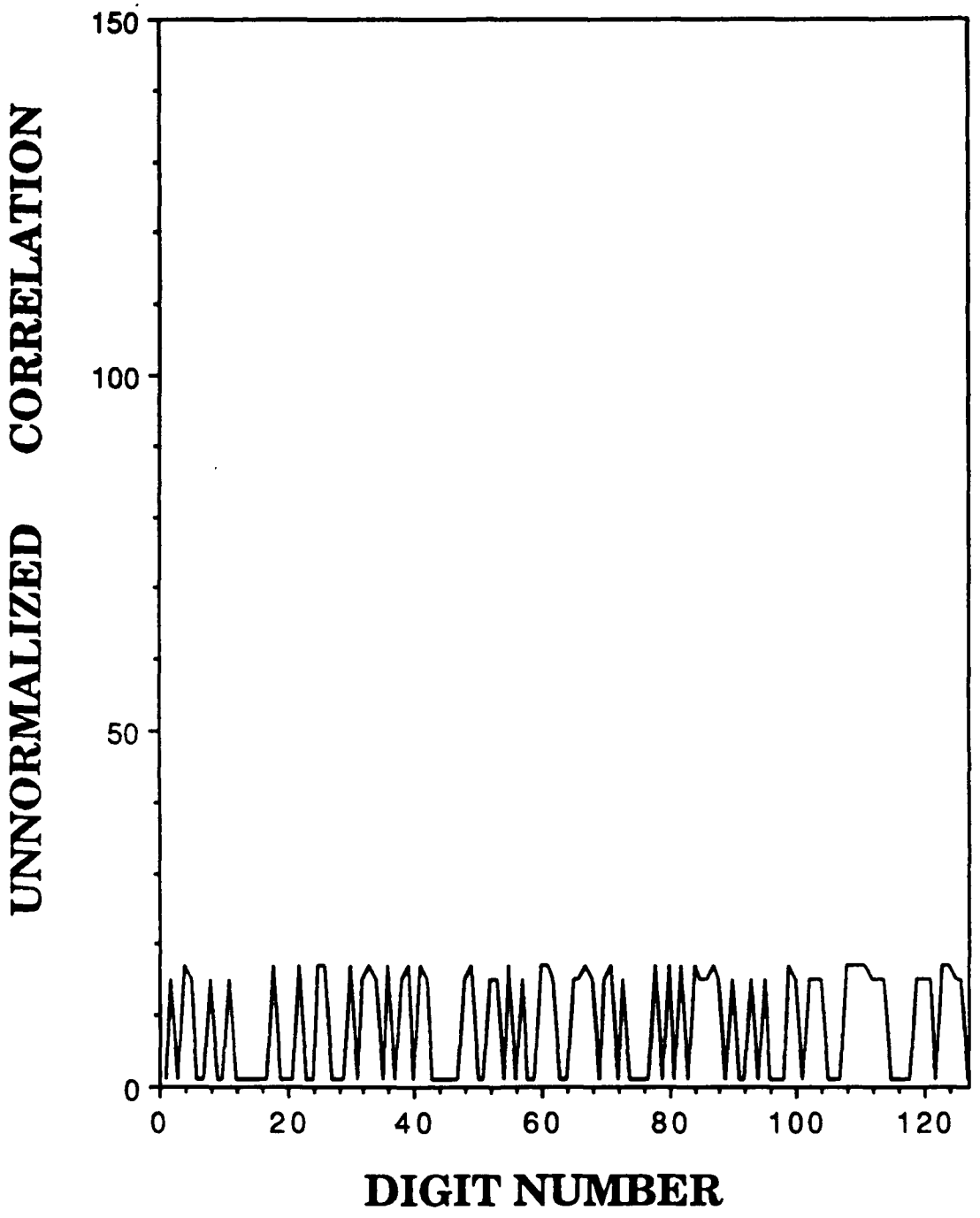

Figure 6. Gold Code Crosscorrelation, N=127.

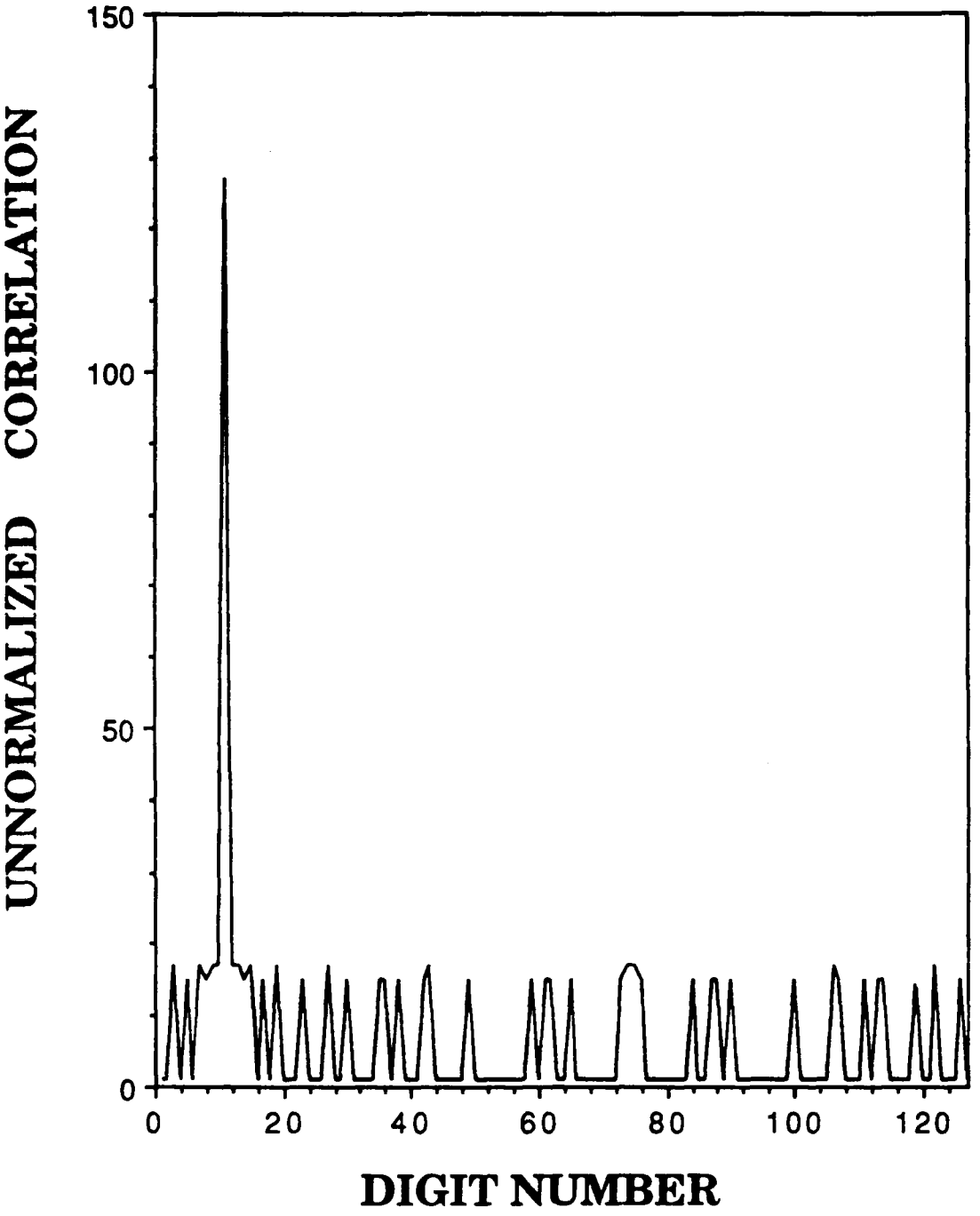

Figure 7. Typical Gold Code Autocorrelation, N=127.

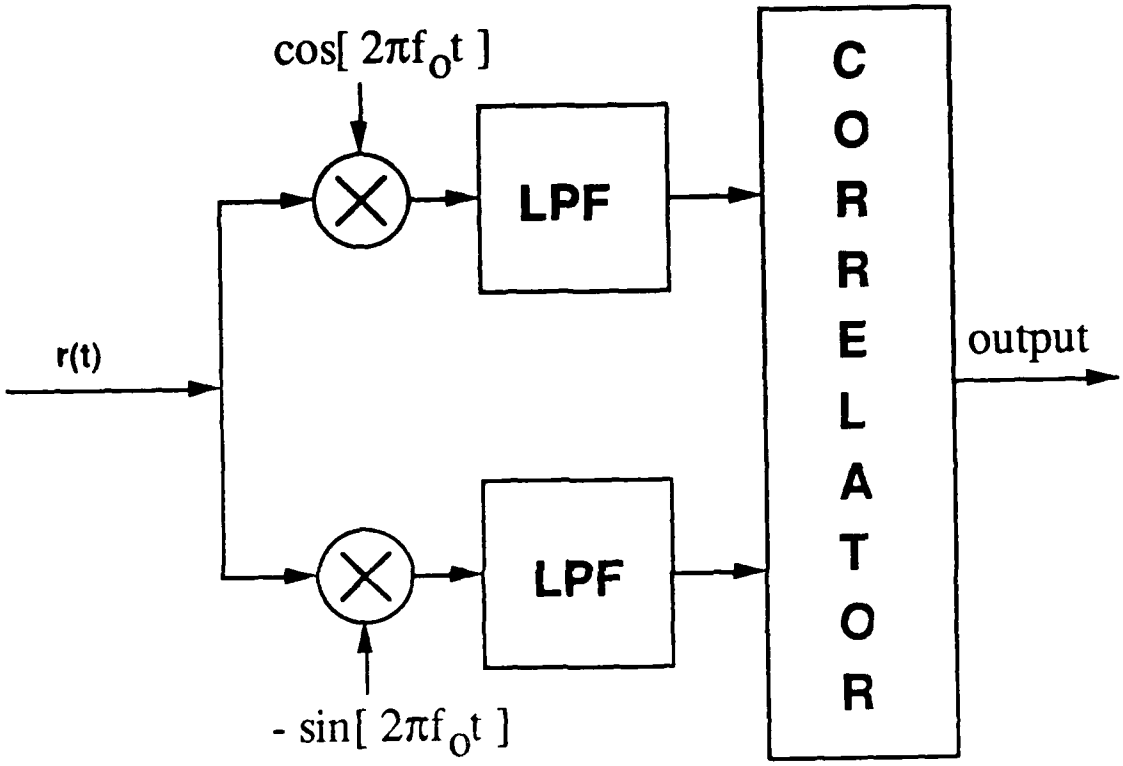

Figure 8. Quadrature Demodulator.

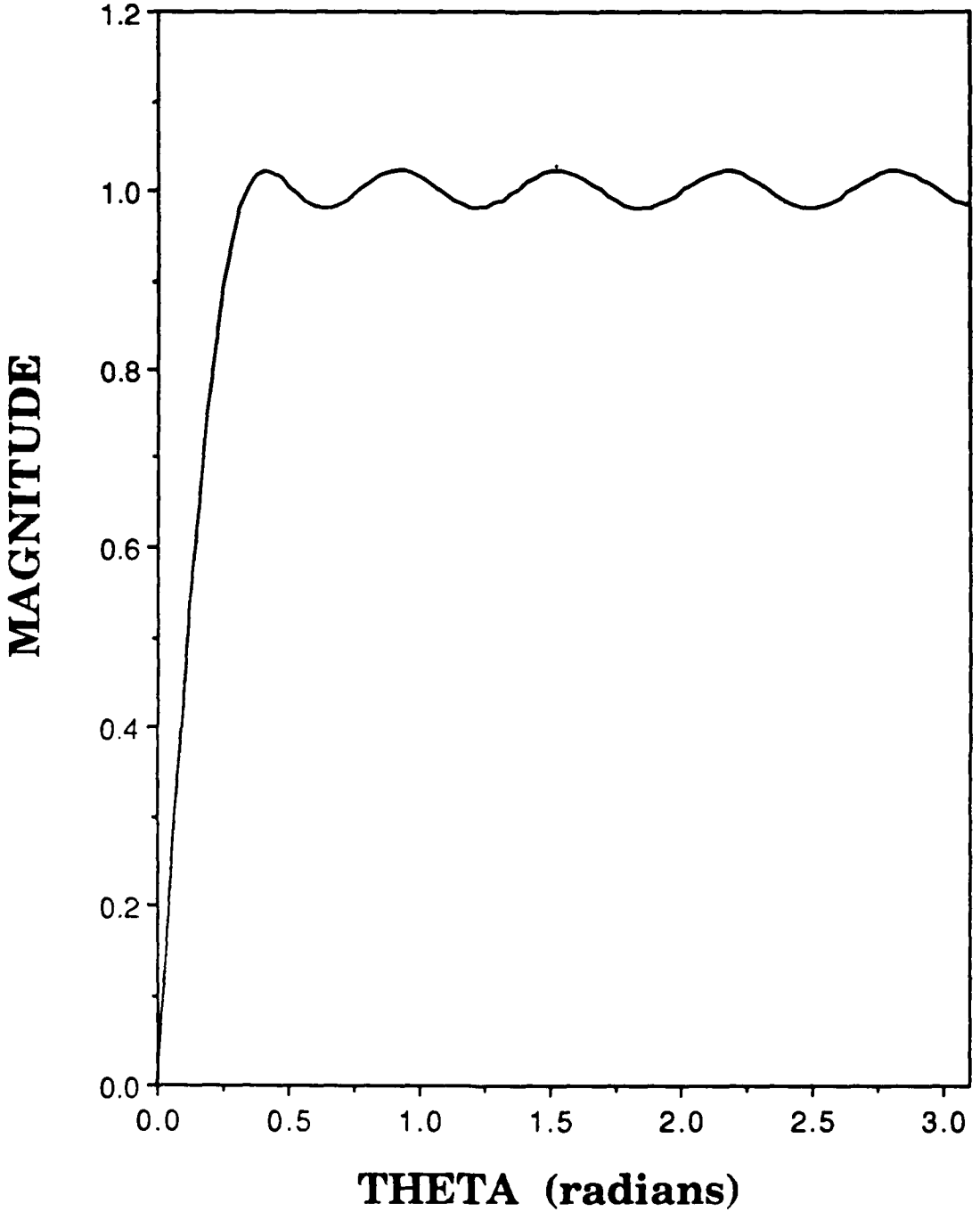

Figure 9. Frequency Response (Magnitude), 19th-Order Digital Hilbert Transformer.

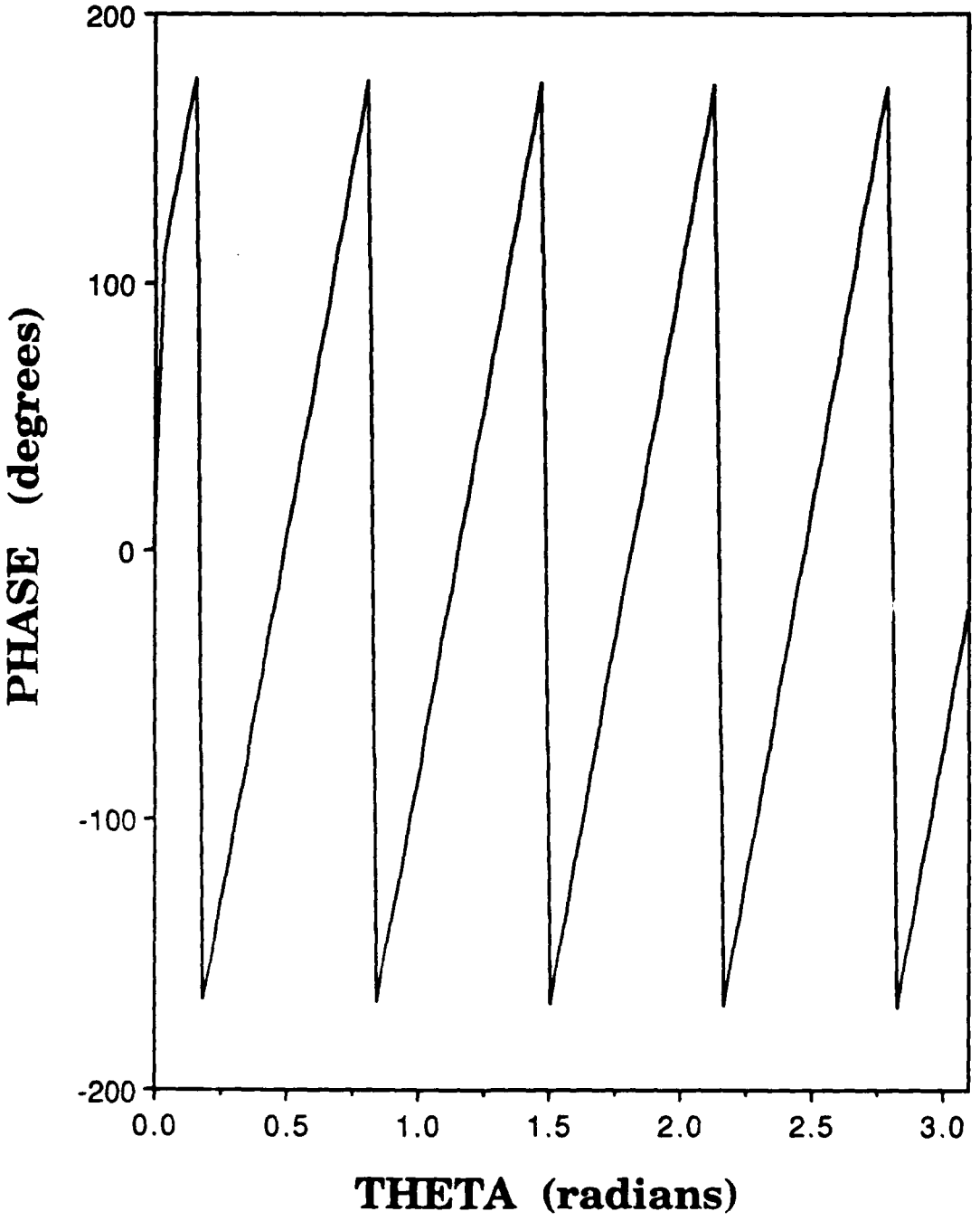

Figure 10. Frequency Response (Phase), 19th-Order Digital Hilbert Transformer.

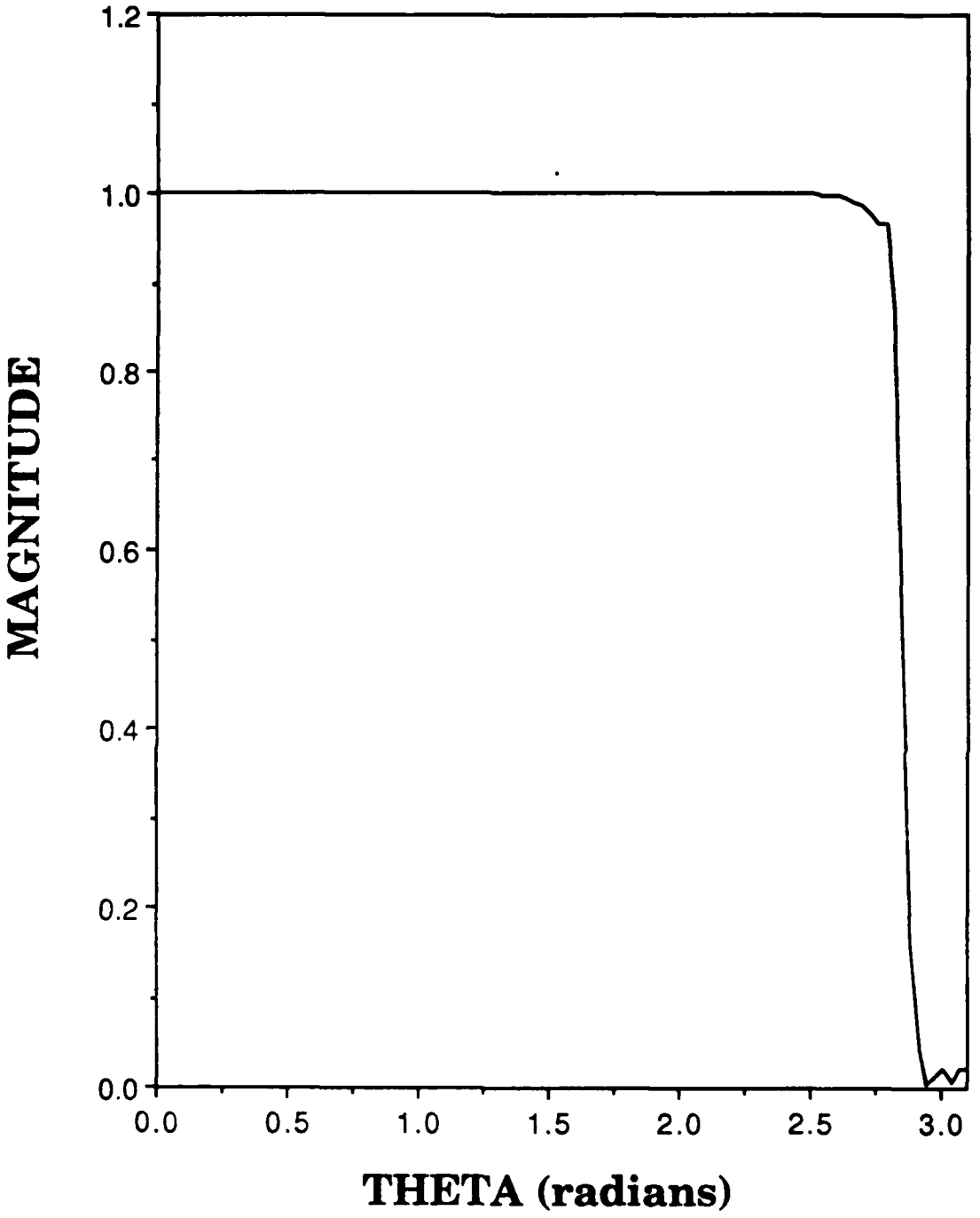

Figure 11. Frequency Response (Magnitude), 8th-Order Butterworth Digital Lowpass Filter.

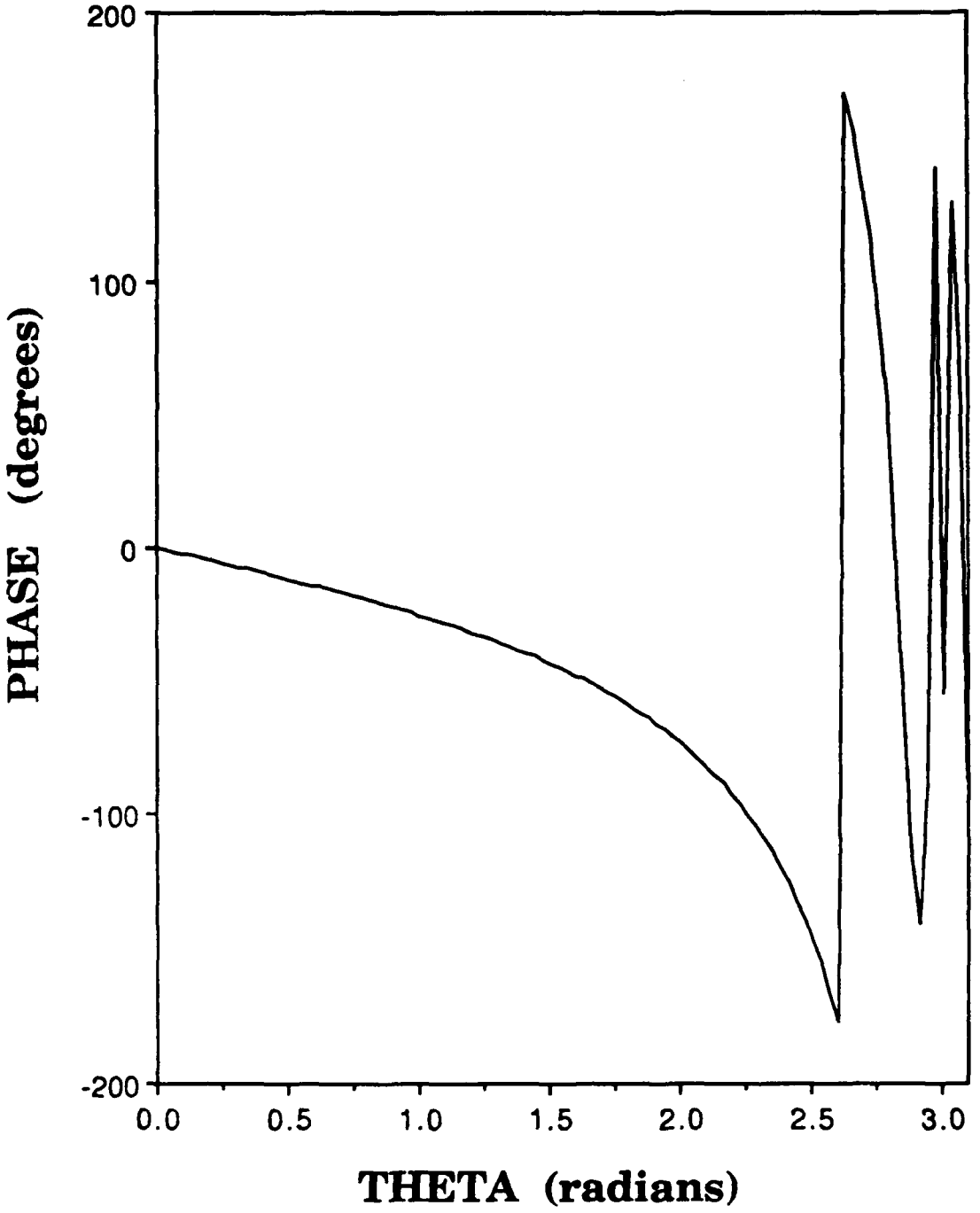

Figure 12. Frequency Response (Phase), 8th-Order Butterworth Digital Lowpass Filter.

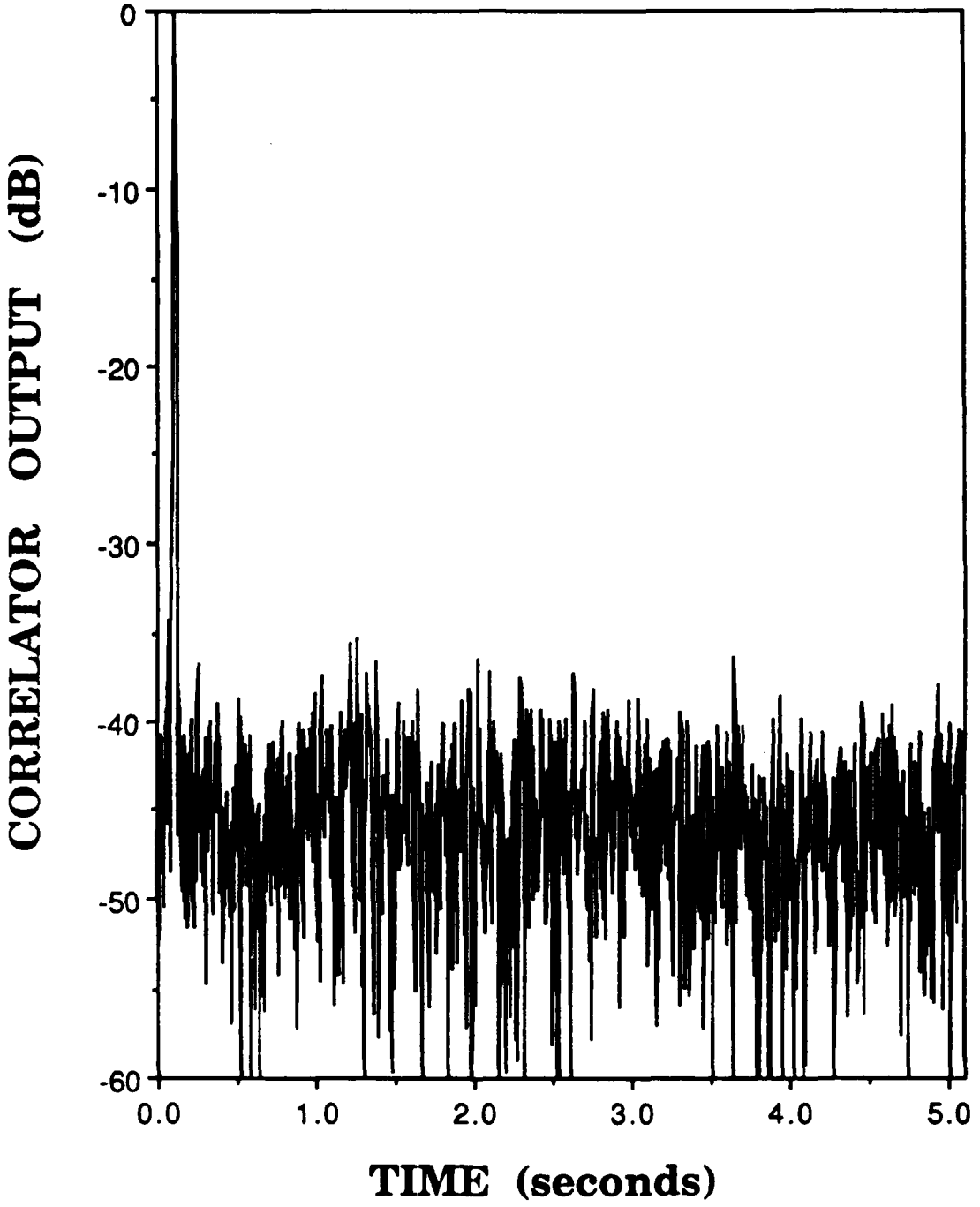

Figure 13. M-Sequence Single-Signal Tomography Results, SNR=0 dB, N=511.

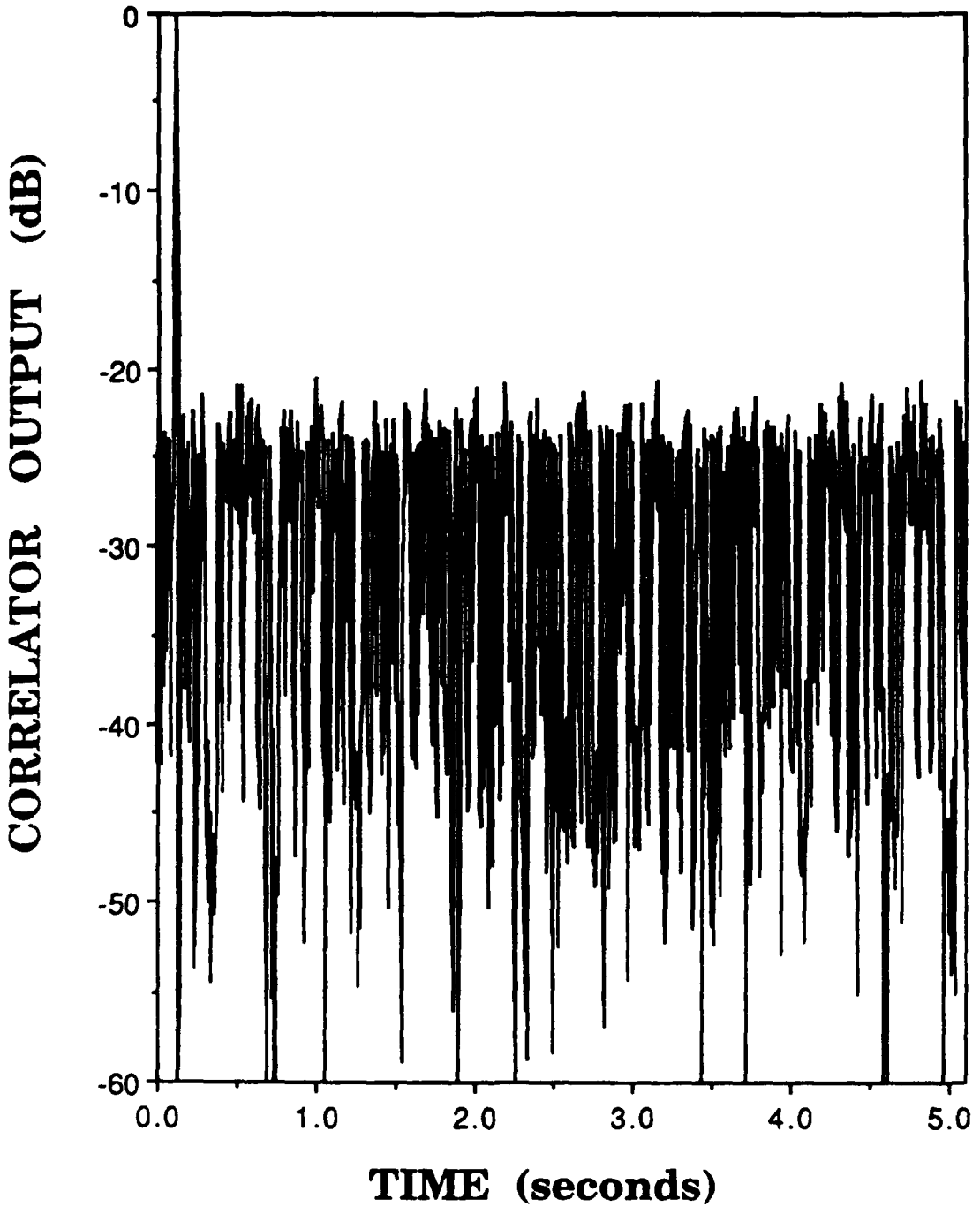

Figure 14. Gold Code Single-Signal Tomography Results, SNR=0 dB, N=511.

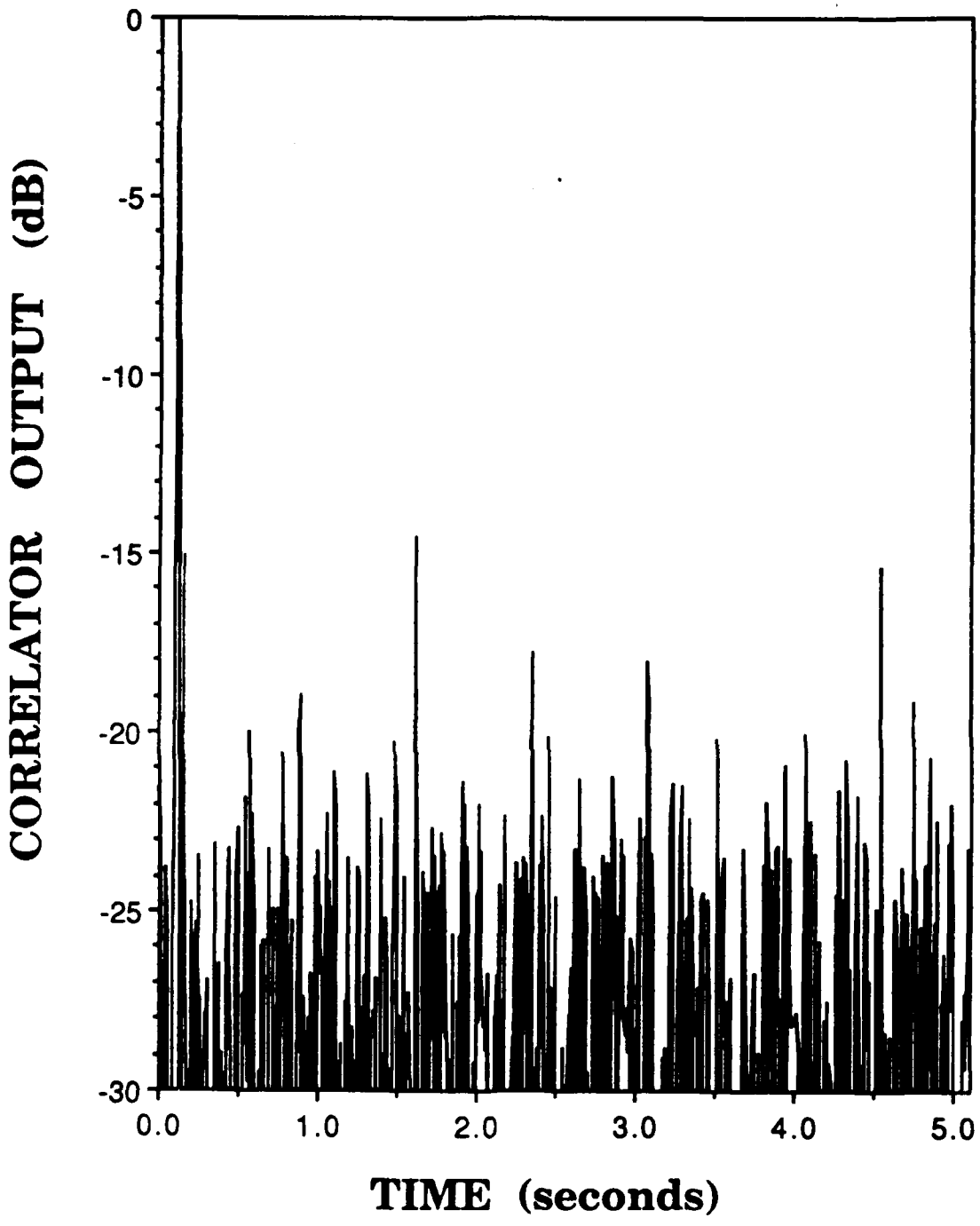

Figure 15. M-Sequence Multi-Signal Tomography Results, No Noise, SJR=0 dB, N=511.

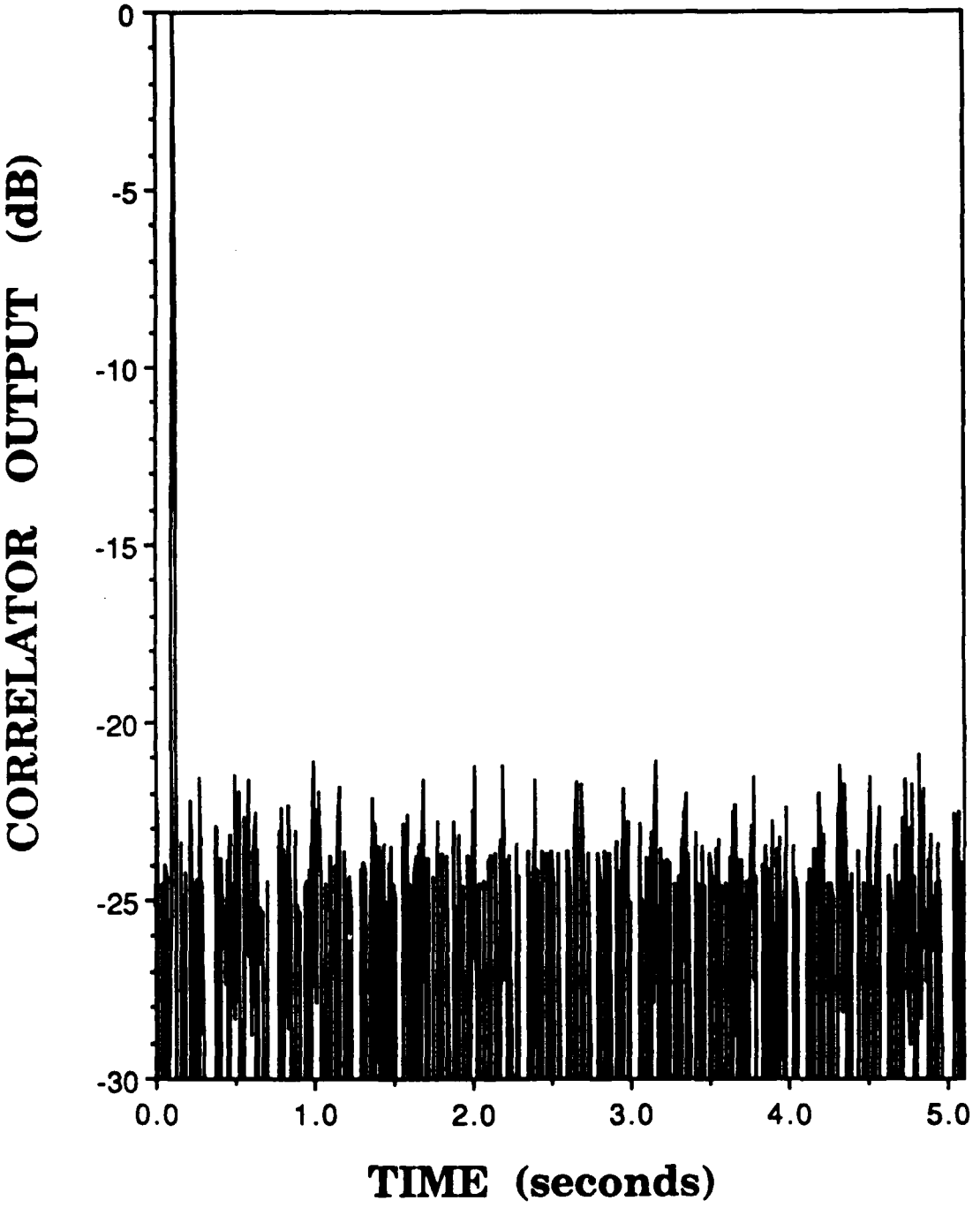

Figure 16. Gold Code Multi-Signal Tomography Results, No Noise, SJR=0 dB, N=511.

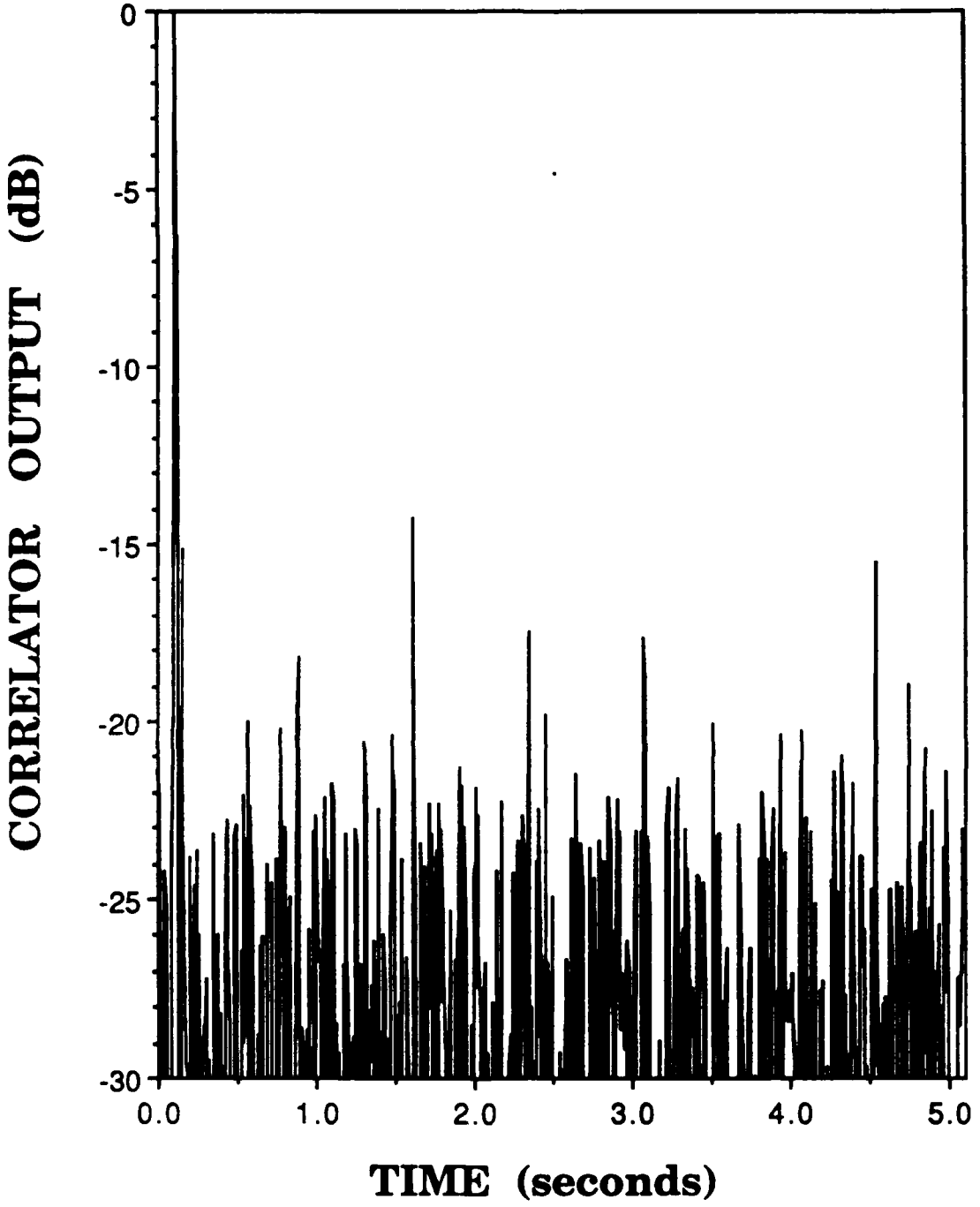

Figure 17. M-Sequence Multi-Signal Tomography Results, SNR=0 dB, SJR=0 dB, N=511.

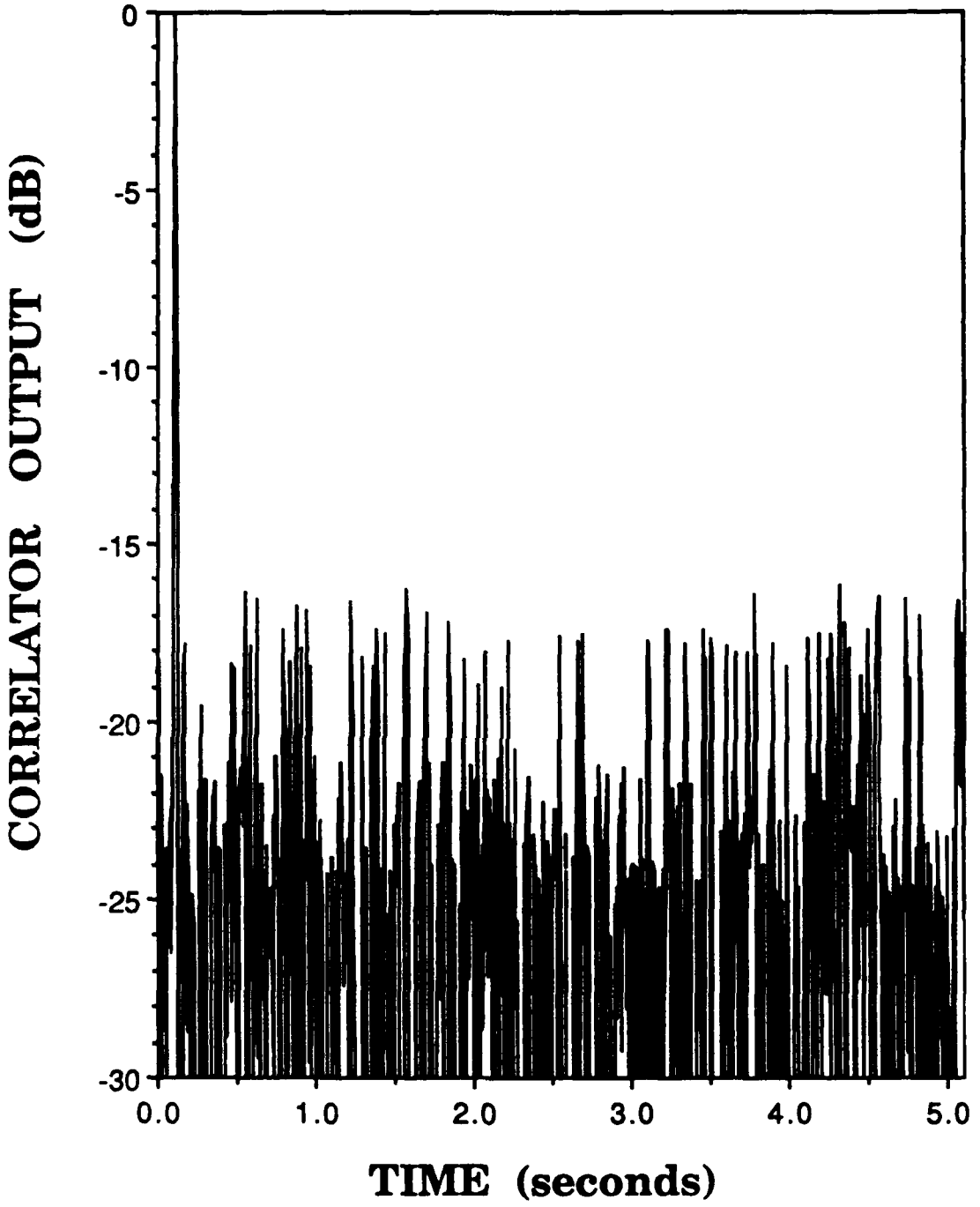

Figure 18. Gold Code Multi-Signal Tomography Results, SNR=0 dB, SJR=0 dB, N=511.

APPENDIX C. DIGITAL HILBERT TRANSFORMER DESIGN

A. SPECIFICATIONS

The purpose of a Hilbert transformer in this simulation was to reproduce the properties of narrowband random processes which additive white Gaussian noise assumes after bandpass filtering. A 19th-order filter (N=20) was chosen to closely approximate this natural phenomenon. This filter design yields a theoretical error of approximately 2.5% This can be verified from Figure 9, by observing that the peak value (1.025) minus the ideal value (1.000) times 100 equals 2.5.

B. THEORY

An ideal Hilbert transform has the following frequency response:

$$H(e^{j\omega}) = \begin{cases} -j, & 0 \le \omega < \pi \\ j, & \pi \le \omega < 2\pi \end{cases} . \qquad \{C1\}$$

The impulse response can be obtained by integration:

$$h(t) = \left[\int_0^{\pi} -je^{j\omega t} d\omega + \int_{\pi}^{2\pi} je^{j\omega t} d\omega \right] . \qquad \{C2\}$$

After evaluating the integrals and replacing t with n for discrete rather than continuous time, the unit sample response becomes

$$h(n) = \begin{cases} 2\sin^2\left(\frac{n\pi}{2}\right), & n \neq 0 \\ 0, & n = 0 \end{cases} . \qquad \{C3\}$$

This idealized Hilbert transformer impulse response has an infinite number of terms, and is therefore unrealizable. Truncating the series of coefficients would eliminate the problem of infinite terms, but simultaneously causes Gibbs phenomenon, representing 9% error near transition points. Moreover, retaining more terms in the truncation will not reduce the Gibbs error; it merely confines it to a more narrow frequency band. Consequently a different approach is used.

The realizable 19th-order (N=20) digital Hilbert transformer utilized was computer-designed by first frequency sampling the ideal frequency response in Equation C1 every $2\pi/N$ radians. Note that the samples so obtained are the DFT coefficients of a filter which has precisely the same frequency response as an ideal Hilbert transform only at the discrete frequencies sampled. For all other frequencies an approximation error occurs. This error is

$$E(e^{j\omega}) = D(e^{j\omega}) - P(e^{j\omega})Q(e^{j\omega}) , \qquad \{C4\}$$

where $D(e^{j\omega})$is the desired ideal frequency response and

$$H^*(e^{j\omega}) = P(e^{j\omega})Q(e^{j\omega}) \qquad \{C5\}$$

is the complex conjugate of the actual frequency response. This error can be minimized by first allowing samples in the transition region (at very low frequency, outside the required passband) to become variables rather than fixed. By expressing P as a linear combination of cosine functions, the problem of minimizing the maximum error between samples becomes a Chebyshev approximation problem. This problem is solved by iteration.

The computer program uses what is known as the Remez algorithm to solve the Chebyshev problem. This solution hinges on the theorem that the best Chebyshev (i.e., weighted sum of r cosines) approximation to a function exhibits r+1 maxima or minima. For the first iteration an initial guess of the r+1 frequencies is made, where for N even, as in this case,

$$r = \frac{N}{2} - 1 \quad , \qquad \{C6\}$$

and the error function is set alternately equal to $+\delta_o$ or $-\delta_o$, where

$$\delta_o = 0.025 \quad , \qquad \{C7\}$$

the theoretical peak error mentioned in Section 1 of this Appendix. This gives rise to r+1 linear equations which are simultaneously solved to obtain new values δ. For each successive iteration δ is used to

interpolate new values for $P(e^{j\omega})$ on the r frequencies sampled. The optimal approximation occurs for

$$\left|E(e^{j\omega})\right| \leq \delta_o \qquad \{C8\}$$

and r+1 extrema. The program iterates until these conditions are met or until 25 iterations are complete. Finally the impulse response coefficients are derived from $P(e^{j\omega})$ as follows:

$$P(e^{j\omega}) = \text{IDFT}\left[P^*(e^{j\omega})\ Q^*(e^{j\omega})\right] . \qquad \{C9\}$$

Inputs to the design problem were the filter length N=20 and the transition band edge 0.05, which represents the range of digital frequency theta

$$0 < \theta \leq 0.3142 , \qquad \{C10\}$$

where the frequency samples are assigned as variables. The output filter coefficients are shown in Table 2. For the actual design program source code and more detailed documentation the reader is referred to Rabiner and Gold [Ref. 12].

C. IMPLEMENTATION

To implement this filter the transfer function was first converted to a difference equation of the following form:

$$y(n) = a_0 x(n) + a_1 x(n-1) + \ldots + a_{19} x(n-19) \quad . \qquad \{C11\}$$

The output sequence y(n) was obtained by iterative computer solution of this difference equation, where the a_i are given in Table 2 [Ref. 13]. Due to filter load time and delay the output (quadrature) noise sequence was ignored for the first twenty samples, and shifted by ten samples thereafter to align with the corresponding input (in-phase) noise sequence.

APPENDIX D. DIGITAL LOWPASS FILTER DESIGN

A. SPECIFICATIONS

The purpose of the lowpass filter in the computer simulation was to reproduce the filtering process used in actual ocean tomography experiments. An 8th-order Butterworth filter was chosen because this is typical in such applications. A cutoff frequency of 90 Hz was also chosen to provide data on a scale comparable to actual tomographic experiments [Ref. 2].

B. THEORY

The analog Butterworth lowpass prototype filter has transfer function

$$H(s) = \frac{1}{1 + a_1 s + a_2 s^2 + \ldots + a_8 s^8} , \qquad \{D1\}$$

where the a_i are from the literature [Ref. 13]. For this application two changes must be made. First, the filter must be converted from analog to digital. Second, the 3 dB cutoff frequency must be converted from an analog normalized frequency of 1.0 to a digital frequency of

$$\theta_c = \frac{2\pi f_c}{f_s} = \frac{2\pi(90)}{200} . \qquad \{D2\}$$

This can be accomplished in one step with the lowpass transformation

$$H(z) = H(s)\Big|_{s = \tan\left(\frac{\theta_c}{2}\right)\frac{z-1}{z+1}} \quad . \qquad \{D3\}$$

Once the substitution in Equation D3 is applied to Equation D1, simplification yields the transfer function and coefficients presented in Table 2.

C. IMPLEMENTATION

This digital filter, like the Hilbert transformer, is implemented by computer solution of its difference equation. In this case, due to terms in the transfer function denominator as well as its numerator, the system is recursive and involves output feedback:

$$y(n) = \sum_{k=1}^{8} a_k\, y(n-k) - \sum_{k=0}^{8} b_k\, x(n-k) \quad , \qquad \{D4\}$$

where in Equation C15 the a_k and b_k are the Butterworth filter coefficients listed in Table 3. Additional information on the design and implementation of this filter can be found in Strum [Ref. 13].

LIST OF REFERENCES

1. Munk, W. and Wunsch, C., "Ocean acoustic tomography: a scheme for large scale monitoring," *Deep-Sea Research*, v. 26A, pp. 123-161, 1979.

2. Spindel, R.C., "Signal Processing in Ocean Tomography", *Adaptive Methods in Underwater Acoustics*, pp. 687-710, 1985.

3. Spindel, R.C., "Ocean Acoustic Tomography: a Review," *Current Practices and New Technology in Ocean Engineering*, v. 11, pp. 7-13, 1986.

4. Gold, R., "Optimal Binary Systems for Spread Spectrum Multiplexing," *IEEE Transactions on Information Theory*, October 1967.

5. Welch, L.R., "Lower Bounds on the Maximum Cross Correlation of Signals," *IEEE Transactions on Information Theory*, May 1974.

6. Ziemer,R.E. and Peterson,R.L., *Digital Communications and Spread Spectrum Systems*, pp. 365-415, Macmillan, 1985.

7. Metzger, K., and Bouwens, R.J., "An Ordered Table of Primitive Polynomials over GF(2) of Degrees 2 Through 19 for Use with Linear Maximal Sequence Generators," TM107, Cooley Electronics Laboratory, University of Michigan, Ann Arbor, July 1972.

8. Birdsall, T.G., Heitmeyer, R.M., and Metzger, K., "Modulation by Linear-Maximal Shift Register Sequences: Amplitude, Biphase and Complement-Phase Modulation," TR216, Cooley Electronics Laboratory, University of Michigan, Ann Arbor, December 1971.

9. Sarwate, D.V. and Pursley, M.B., "Crosscorrelation Properties of Pseudorandom and Related Sequences," *Proceedings of the IEEE*, v. 68, No. 5, pp. 593-619, May 1980.

10. Sarwate, D.V., "Bounds on Crosscorrelation and Autocorrelation of Sequences," *IEEE Transactions on Information Theory*, v. IT- 25, No. 6, pp. 720-724, November 1979.

11. Peebles, P.Z., *Probability, Random Variables, and Random Signal Principles*, second edition, pp. 220-226, McGraw-Hill, 1987.

12. Rabiner, L.R. and Gold, B., *Theory and Application of Digital Signal Processing*, pp. 192-193, Prentice-Hall, 1975.

13. Strum, R.D. and Kirk, D.E., *First Principles of Discrete Systems and Digital Signal Processing*, pp. 611-719, Addison-Wesley, 1988.

INITIAL DISTRIBUTION LIST

	No. Copies
1. Defense Technical Information Center Cameron Station Alexandria, VA 22304-6145	2
2. Library, Code 0142 Naval Postgraduate School Monterey, CA 93943-5002	2
3. Prof. James H. Miller, Code 62Mr Dept. of Electrical and Computer Engineering Naval Postgraduate School Monterey, CA 93943-5000	15
4. Prof. Lawrence J. Ziomek, Code 62Zm Dept. of Electrical and Computer Engineering Naval Postgraduate School Monterey, CA 93943-5000	1
5. Dr. James F. Lynch Woods Hole Oceanographic Institution Woods Hole, MA 02543	1
6. Prof. Ching-Sang Chiu, Code 68Ci Dept. of Oceanography Naval Postgraduate School Monterey, CA 93943-5000	1
7. Chairman, Code 62 Dept. of Electrical and Computer Engineering Naval Postgraduate School Monterey, CA 93943-5000	1